Highly chirped single-bandpass microwave photonic filter with reconfiguration capabilities

Mario Bolea,* José Mora, Beatriz Ortega and José Capmany

ITEAM Research Institute, Universidad Politécnica de Valencia,C/ Camino de Vera, s/n 46022 Valencia, Spain
*mabobo1@iteam.upv.es

Abstract: We propose a novel photonic structure to implement a chirped single-bandpass microwave photonic filter based on the amplitude modulation of a broadband optical signal transmitted by a non-linear dispersive element and an interferometric system prior to balanced photodetection. A full reconfigurability of the filter is achieved since amplitude and phase responses can be independently controlled. We have experimentally demonstrated chirp values up to tens of ns/GHz, which is, as far as we know, one order of magnitude better than others achieved by electrical approaches and furthermore, without restrictions in terms of frequency tuning since a frequency operation range up to 40 GHz has been experimentally demonstrated.

©2011 Optical Society of America

OCIS codes: (060.0060) Fiber optics and optical communications; (060.5625) Radio frequency photonics.

References and links

1. J. Capmany, and D. Novak, "Microwave photonics combines two worlds," Nat. Photonics **1**(6), 319–330 (2007).
2. J. Yao, "Microwave photonics," J. Lightwave Technol. **27**(3), 314–335 (2009).
3. J. Capmany, B. Ortega, D. Pastor, and S. Sales, "Discrete-Time optical processing of microwave signals," J. Lightwave Technol. **23**(2), 702–723 (2005).
4. J. Capmany, B. Ortega, and D. Pastor, "A tutorial on Microwave Photonic Filters," J. Lightwave Technol. **24**(1), 201–229 (2006).
5. M. A. G. Laso, T. Lopetegi, M. J. Erro, D. Benito, M. J. Garde, M. A. Muriel, M. Sorolla, and M. Guglielmi, "Real-Time spectrum analysis in microstrip technology," IEEE Trans. Microw. Theory Tech. **51**(3), 705–717 (2003).
6. J. D. Schwartz, J. Azaña, and D. V. Plant, "A Fully Electronic System for the Time Magnification of Ultra-Wideband Signals," IEEE Trans. Microw. Theory Tech. **55**(2), 327–334 (2007).
7. G. N. Saddik, R. S. Singh, and R. Brown, "Ultra-wideband multifunctional communications/radar system," IEEE Trans. Microw. Theory Tech. **55**(7), 1431–1437 (2007).
8. R. S. Withers, A. C. Anderson, P. V. Wright, and S. A. Reible, "Superconductive tapped delay lines for microwave analog signal processing," IEEE Trans. Magn. **19**(3), 480–484 (1983).
9. F. Huang, "Low loss quasitransversal microwave filters with specified amplitude and phase characteristics," Proc. Inst. Electr. Eng. **140**, 433–440 (1993).
10. F. Huang, "Quasitransversal synthesis of microwave chirped filters," Electron. Lett. **28**(11), 1062–1064 (1992).
11. T. Lopetegi, M. A. G. Laso, J. Hernandez, M. Bacaicoa, D. Benito, M. J. Garde, M. Sorolla, and M. Guglielmi, "New microstrip "Wiggly-Line" filters with spurious passband supression," IEEE Trans. Microw. Theory Tech. **49**(9), 1593–1598 (2001).
12. M. A. G. Laso, T. Lopetegi, M. J. Erro, D. Benito, M. J. Garde, M. A. Muriel, M. Sorolla, and M. Guglielmi, "Chirped delay lines in microstrip Technology," IEEE Trans. Microw. Wireless Compon. Lett. **11**(12), 486–488 (2001).
13. J. D. Schwartz, J. Azaña, and D. V. Plant, "Experimental demonstration of real-time spectrum analysis using dispersive microstrip," IEEE Trans. Microw. Wireless Compon. Lett. **16**(4), 215–217 (2006).
14. J. D. Schwartz, I. Arnedo, M. A. G. Laso, T. Lopetegi, J. Azaña, and D. V. Plant, "An electronic UWB continuously tunable time-delay system with nanosecond delays," IEEE Trans. Microw. Wireless Compon. Lett. **18**(2), 103–105 (2008).
15. J. D. Schwartz, R. Abhari, D. V. Plant, and J. Azaña, "Design and analysis of 1-D uniform and chirped electromagnetic bandgap structures in substrate-integrated waveguides," IEEE Trans. Microw. Theory Tech. **58**(7), 1858–1866 (2010).
16. J. Mora, B. Ortega, A. Díez, J. L. Cruz, M. V. Andrés, J. Capmany, and D. Pastor, "Photonic microwave tunable single-bandpass filter based on a Mach-Zehnder Interferometer," J. Lightwave Technol. **24**(7), 2500–2509 (2006).

17. S. Wakabayashi, and A. Baba, "Design and fabrication of an apodization profile in linearly chirped fiber Bragg gratings for wideband > 35 nm and compact tunable dispersion compensator," Appl. Opt. **19**, 1653–1660 (1980).

1. Introduction

Microwave photonics can be considered a research area where microwave and optical fields converge. The different topics covered by microwave photonics are focused on photonic generation, processing, control and distribution of microwave and millimeter-wave signals. The main interest on microwave photonics lies in the use of photonic technologies to provide functions in microwave systems that are very complex or even impossible to be carried out directly in the radiofrequency (RF) domain. Nevertheless, the great potential of microwave photonics is achieved in Radio-over-Fiber (RoF) systems since it profits from the fiber advantages for the transport and distribution of RF signal such as: low loss, high bandwidth, immunity to electromagnetic interference (EMI) and the possibility of tuning and reconfiguration [1,2].

Photonic signal processing has attracted a special interest due to the capacity to operate with microwave, millimeter-wave and RF signals free from bandwidth constraint [3]. Moreover, in a RoF environment, the signal processing directly in the optical domain avoids the need of electro-optical and opto-electrical conversions. Microwave photonic filters can be considered as the key element in processing and control systems. Most of the proposed systems in the literature to implement microwave photonic filters are focused on modifying the amplitude response without exploiting the phase characteristics [4]. Nevertheless, the use of filters with dynamic and/or non constant group delay arises great interest in applications where signal processing not only involves the signal amplitude control. In this sense, chirped filters typically present a flat magnitude and quadratic phase characteristic i.e. the delay follows a linear behaviour characterized by a certain slope within the passband [5]. This kind of filters has become valuable components in applications which require a careful control over signal temporal characteristics such as high-performance radar, Ultra-Wideband communications and spectral analysis systems involving high bandwidth signal processing [5–7].

In the literature, several approaches in the electrical domain have been proposed to implement chirped delay line filters. Firstly, surface acoustic wave (SAW) devices were proposed as chirped delay lines implemented on stripline [8,9] and coplanar line [10] structures. Nevertheless, these technologies were limited to a few gigahertz frequency operation range and exhibited high propagation losses. During the last decade, chirped electromagnetic-bandgap (EBG) structures in microstrip technology operating in reflective mode have been also proposed [11, 12]. Their experimental implementation have been demonstrated for a fixed [5, 13] and tunable [14] electrical group-delay time. Nevertheless, the frequency operation range of these devices is restricted to 15 GHz with a maximum group delay slope of 2 ns/GHz due to the excessive losses over long distances [6]. In order to achieve higher frequencies, substrate integrated waveguides (SIW) have been recently proposed to implement EBG structures which extend the operation frequency range up to several tens of gigahertz [15], although the group-delay slope only achieves 0.2 ns/GHz as a maximum value. In this sense, the implementation of chirped filters in optical domain becomes a promising solution thanks to the higher frequency operation range and flexibility demonstrated by microwave photonics.

In this paper, a photonic architecture to implement a chirped single bandpass filter is presented which is fully reconfigurable both in terms of amplitude and phase response. Different capabilities of the system are experimentally demonstrated related to the control of the frequency tuning, the amplitude response and the group delay time slope over the electrical transfer function. The structure is based on the amplitude modulation of a broadband source which is chirped through a non-linear dispersive element and sliced by a Mach-Zehnder Interferometer prior to the balanced photodetection. In this way, the paper is organized as follows: In section 2, we provide a system description through a qualitative analysis to explain the filter operation principle with the basic design rules to achieve the

desired characteristics. Section 3 shows the experimental system behaviour demonstrating the control over the central frequency, the amplitude response shape and the chirp. Finally, in section 4, we summarize the most important results obtained in this paper.

2. Theoretical background

Figure 1 shows the block diagram of the proposed chirped single bandpass filter. Firstly, a broadband optical signal, whose power spectral distribution can be properly adjusted, is amplitude modulated by a RF-signal in an external electrooptical modulator (EOM). The modulated signal is launched into a nonlinear dispersive element which can be characterized as a phase filter whose optical transfer function is given by:

$$H_{OPT}(\omega) = e^{j\varphi(\omega)} \tag{1}$$

where ω corresponds to the angular optical frequency. Phase dependence can be developed by means of a Taylor expansion around the central frequency of the optical source ω_0 [16]:

$$\varphi(\omega) = \varphi_0 + \dot\varphi_0 \cdot (\omega - \omega_0) + \frac{1}{2!}\ddot\varphi_0 \cdot (\omega - \omega_0)^2 + \frac{1}{3!}\dddot\varphi_0 \cdot (\omega - \omega_0)^3 \tag{2}$$

where $\dot\varphi_0$ is the group-delay time at the central optical frequency ω_0 and $\ddot\varphi_0$ and $\dddot\varphi_0$ are the first order dispersion and the dispersion slope, respectively, evaluated at the same frequency.

The optical signal undergoes a group delay time through the dispersive element which can be obtained from Eq. (2) by means of the first order derivative:

$$\tau_{OPT}(\omega) = \frac{d\varphi(\omega)}{d\omega} = \dot\varphi_0 + \ddot\varphi_0 \cdot (\omega - \omega_0) + \frac{1}{2}\dddot\varphi_0 \cdot (\omega - \omega_0)^2 \tag{3}$$

Following a new derivative order from Eq. (3), the dispersion dependence on the optical frequency is given by:

$$\ddot\varphi(\omega) = \frac{d\tau_{OPT}(\omega)}{d\omega} = \ddot\varphi_0 + \dddot\varphi_0 \cdot (\omega - \omega_0) \tag{4}$$

At the output of the nonlinear dispersive element, a Mach-Zehnder Interferometer (MZI) slices the optical spectrum and allows to obtain the different filter taps with a continuous and sinusoidal transfer function $T(\omega)$ described as:

$$T(\omega) = \frac{1}{2}\left[1 + \cos\left(2\pi \cdot \frac{\omega - \omega_0}{\Delta\omega}\right)\right] \quad with \quad \Delta\omega = \frac{2\pi}{\Delta\tau} \tag{5}$$

where $\Delta\omega$ corresponds to the periodicity of the MZI transfer function and $\Delta\tau$ is the optical delay introduced between both arms.
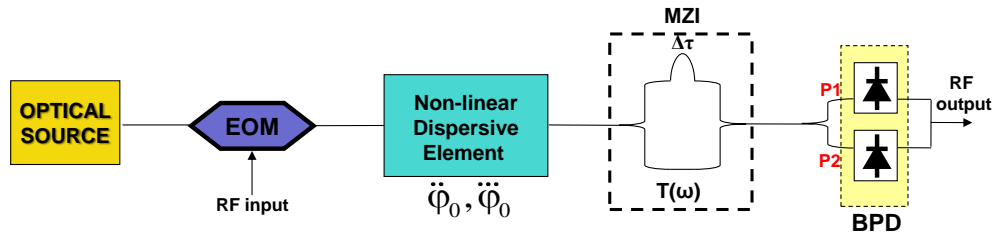

Fig. 1. Block diagram of chirped filter based on a single bandpass photonic filter with differential detection.

Finally, signal detection is done by means of a balanced photodetector (BPD) whose input ports, P1 and P2, are connected with both MZI output arms. This device realizes the electrical subtraction of the signal detected in both ports to obtain the system transfer function.

A complete theoretical analysis of the structure permits to obtain an approximation of the central frequency of the filter passband related to the MZI slicing and the induced dispersion. In this way, the central frequency of passband ($\Omega_i = 2\pi \cdot f_i$) can be approximated by [16]:

$$f_i = \frac{\Delta\tau}{2\pi \cdot \left|\ddot{\varphi}(\omega_i)\right|} \tag{6}$$

where ω_i represents the angular optical frequency in which is centred the optical source.

In order to understand the system behaviour, we are going to carry out a qualitative analysis making use of numerical simulations whose main results are shown in Fig. 2.

Firstly, a uniform optical source is selected with a $\delta\omega'$ bandwidth of 0.5 THz centred at ω_1 optical frequency of 191.5 THz (Fig. 2a), a dispersive element characterized by $\ddot{\varphi}_0 = -500 \; ps^2$ and $\dddot{\varphi}_0 = 2.5 \; ps^3$, and an optical delay ($\Delta\tau$) between MZI arms around 20π ps. As a result, an electrical transfer function with a passband around f_1 is obtained as can be observed in Fig. 2d. When the source is centred at 196 THz (ω_2) (Fig. 2b), the central frequency of the passband is placed around f_2 since dispersion value is different according to Eq. (6), as can be confirmed in the electrical transfer function (Fig. 2e).

If the optical source width is increased up to $\delta\omega = 10 \cdot \delta\omega'$ and centred at $\omega_0 = (\omega_1 + \omega_2)/2$ (Fig. 2c), the passband is wider than previous cases and tuned around $f_0 = (f_1 + f_2)/2$ as it is shown in Fig. 2f. The bandwidth of the passband is related to the difference between frequencies f_1 and f_2 (Δf) which, from Eqs. (4) and (6), can be approximated by:

$$\Delta f = f_2 - f_1 \approx -f_0 \cdot \delta\omega \cdot \frac{\dddot{\varphi}_0}{\ddot{\varphi}_0} \tag{7}$$

Note that Δf is linearly dependent on the optical source bandwidth $\delta\omega$ through a scale factor which is related to the ratio between the dispersion parameters. The frequency f_0 corresponds to the central frequency of the passband when optical source is centred at ω_0 according to Eq. (6).

We also pay attention to the electrical group-delay time obtained in each case. In Fig. 2g, we plot the electrical group-delay when the optical sourced is centred at ω_1. As can be observed, it keeps a constant value (τ_1) within the passband. On the other hand, when the optical source is centred at ω_2 the electrical group-delay time also presents a constant value of τ_2 within the passband (Fig. 2h). In both cases, an asymmetry is found out of band which is due the effects of second order dispersion over the electrical transfer function.

In order to show the chirp characteristics of the system, the source is extended to cover the whole optical bandwidth $\delta\omega$ giving an electrical group-delay time which presents a linear behaviour within the passband from τ_1 and τ_2 as can be observed in Fig. 2i. We can obtain from Eq. (3) the electrical group-delay $\Delta\tau_{RF}$ between the passband centred at f_1 and f_2 which is given by:

$$\Delta\tau_{RF} = \tau_{OPT}(\omega_2) - \tau_{OPT}(\omega_1) = \ddot{\varphi}_0 \delta\omega \tag{8}$$

Note that the electrical group-delay $\Delta\tau_{RF}$ corresponds to the difference optical delay produced in the dispersive element. Thereby, according to the results shown in Fig. 2, the passband generated can be understood as the addition of all the single passband produced around f_i with an electrical group-delay τ_i from the infinitesimal optical source components centred at ω_i.

Additionally, we can find the chirp (C) as the electrical group-delay slope within the passband related to the Eqs. (7) and (8):

$$C = \frac{\Delta\tau_{RF}}{\Delta f} \approx -\frac{\ddot{\varphi}_0^2}{f_0 \cdot \dddot{\varphi}_0} \qquad (9)$$

From Eq. (9), we can observe that the chirp effect within the passband is a consequence of the use of a nonlinear dispersive element presenting a dispersion slope $\dddot{\varphi}_0$ which affects the whole optical source spectrum. Note that the sign of the chirp C is determined by the parameter $\dddot{\varphi}_0$ of the dispersive element.
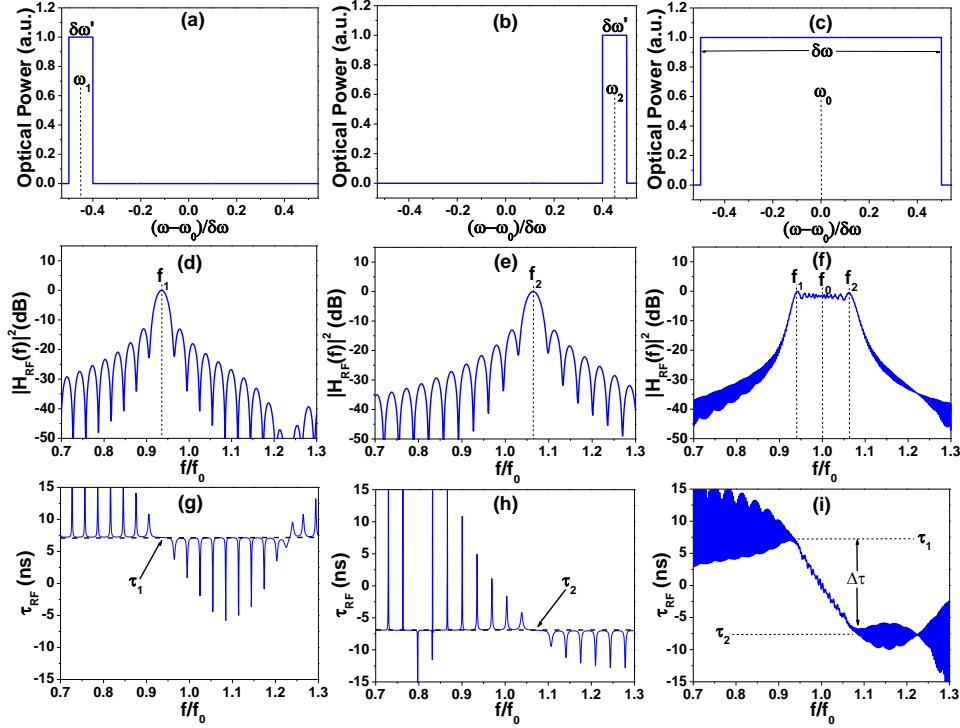

Fig. 2. Uniform optical source power distribution with a central optical frequency and a bandwidth of (a) ω_1 and $\delta\omega'$, (b) ω_2 and $\delta\omega'$ and (c) ω_0 and $\delta\omega$; (d), (e) and (f) and (g), (h) and (i) are the amplitude response and electrical group-delay time, respectively, corresponding to each optical source case.

We have shown the capacity to generate a linearly chirped filter as a novelty respect to other photonic structures in the literature [3,4] which do not exploit the phase characteristics of filters. Furthermore, our system presents more advantages which make it even more attractive, such as to avoid the Carrier Suppression Effect (CSE) and to remove the baseband component. In order to show these properties a numerical simulation is carried out in Fig. 3 using a 4.8 THz width uniform profile of optical source, a dispersive element characterized by $\dddot{\varphi}_0 = -127\ ps^2$ and an optical delay ($\Delta\tau$) for the MZI of 20 ps for tuning the filter passband at 25 GHz. Note that the first notch of the CSE (dashed line) is located at the design frequency of the filter (solid line). Ideally, CSE affects to the transfer function of photonic systems when Double-Side-Band (DSB) modulation is used reducing the frequency operation range of the system [16]. However, Fig. 3 shows an electrical transfer function $|H_{RF}(f)|^2$ of the designed filter which is free from the destructive interference related to the first notch of the CSE. Therefore, we can observe that our approach avoids the CSE as a consequence of the employed interferometric structure. Alternative modulation as Single-Side-Band (SSB) modulation can be used to eliminate the CSE but the complexity of the system is increased and the operation is limited at high frequencies. However, our all-optical proposal has an

unlimited operation bandwidth and experimentally the operation range is only conditioned by the electro-optical components.

On the other hand, as we can observe in Fig. 3, the baseband component of the filter transfer function has been removed due to the use of balanced photodetection and a single bandpass filter has been achieved. Many structures proposed in the literature increase their complexity in order to remove the baseband component by means of the implementation of negative coefficients of the filter [3,4]. As demonstrated above, our structure allows to benefit from these advantages without an increasing the system complexity.
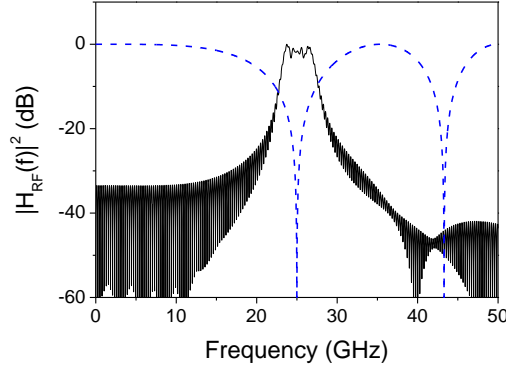
Fig. 3. Amplitude response system for passband tuned at 25 GHz (solid line) and carrier suppression effect due to the dispersion $\ddot{\varphi}_0$ (dashed line).

3. Experimental setup

In this section, the main capabilities filter proposed to achieve a full reconfiguration are experimentally demonstrated. Figure 4 shows the experimental architecture of the system. The optical source can be reconfigured to obtain different optical power distribution profiles. It is composed by an 80 nm ASE source as Broadband Source (BBS) and a 48-channel optical channel selector (OCS) centered at 1546.92 nm with 0.8 nm channels width. The attenuation of each channel can be independently controlled and therefore, the spectral power distribution can be reconfigured to obtain the desired profile. The optical signal is DSB amplitude modulated by a RF-signal generated by a microwave networks analyzer Agilent E8364A in an external Mach-Zehnder Modulator (MZM) operating in the linear region. The modulated signal is introduced in a standard single mode fiber link SMF-28 with a length of L which is used as a broadband dispersive element characterized by $\ddot{\varphi}_0 = \beta_2 L \ and \ \dddot{\varphi}_0 = \beta_3 L$ where β_2 and β_3 are optical fiber intrinsic parameters with values of −21 ps²/Km· and 0.13 ps³/Km. The optical signal at the end of the fiber link is driven to a MZI based on two 50/50 couplers and a Variable Delay Line (VDL) placed in one of the interferometer arms to control the time delay difference (Δτ) between the both arms. The two optical signals at the output of the MZI are launched into ports 1 (P1) and 2 (P2) of a BPD, with a 50 GHz bandwidth. The resulting system transfer function, $H_{RF}(f)$, is displayed by a microwave networks analyzer.

OCS

BBS

OPTICAL SOURCE

RF input

MZM

SMF

$$\ddot{\varphi}_0 = \beta_2 L$$
$$\dddot{\varphi}_0 = \beta_3 L$$

MZI

$\Delta\tau$

VDL

50/50 Couplers

P1

P2
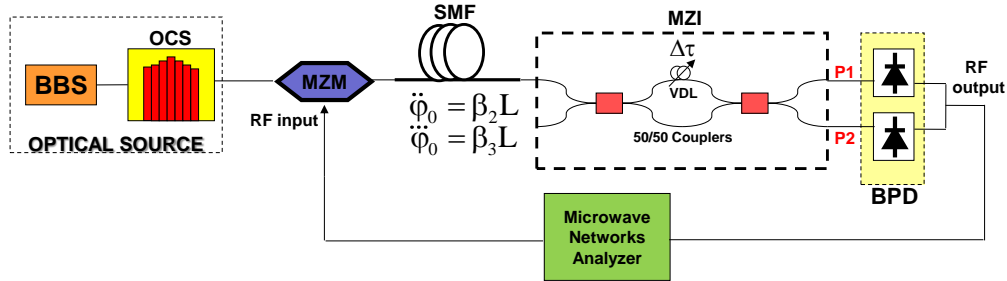
BPD

RF output

Microwave
Networks
Analyzer

Fig. 4. Experimental layout of the chirped filter.

In order to show the system performance, different chirped passbands have been implemented and main results are plotted in Fig. 5. The optical source was adjusted to generate a 38.4 nm width uniform profile by means of the OCS, the dispersion was $\ddot{\varphi}_0 = -1050 \; ps^2$ and the time delay difference ($\Delta\tau$) of the MZI was set at 199.4 psec for tuning the passband at 30 GHz according to Eq. (6). Figure 5a shows the amplitude response, $|H_{RF}(f)|^2$, and electrical group-delay time, τ_{RF}, of the microwave filter. The 10-dB bandwidth of the passband is around 5.83 GHz and the electrical group-delay within this band presents a linear behaviour with a slope of −5.61 ns/GHz. Figure 5b shows the amplitude response and the electrical group-delay time when the optical source bandwidth was reduced to 19.2 nm. In this case, the electrical group-delay maintains the linear behaviour with a slope of −5.48 ns/GHz similar to the previous one and 10-dB bandwidth is around 2.3 GHz which is half the of the one in Fig. 5a, according to Eq. (7). Figure 5c shows the obtained amplitude response and electrical group-delay time when the dispersion was set to $\ddot{\varphi}_0 = -525 \; ps^2$, and the MZI time delay difference was adjusted to 99 ps to maintain the passband centered around 30 GHz. In this case, the 10-dB bandwidth of the passband is around 5.78 GHz is similar to Fig. 5a. Nevertheless, the slope of the electrical group-delay time within the passband is −2.72 ns/GHz according to the Eq. (9) since total dispersion introduced by the optical fiber link has been reducing to half. Finally, using the same parameters employed in measurements displayed in Fig. 5c, the central frequency of the passband (f_0) was moved to 15 GHz by means of setting $\Delta\tau$ to 48 ps. As can be observed, the electrical group-delay time has a linear slope of −5.45 nsec/GHz what is similar to the slope obtained in Fig. 5a and 5b. However, 10-dB bandwidth is reduced to 2.4 GHz, which is approximately half of the value shown in Fig. 5a and 5b, also from Eq. (7). Theoretical results generated by numerical simulations have been included in Fig. 5 using of dashed lines and we note the excellent agreement between them and the experimental results.
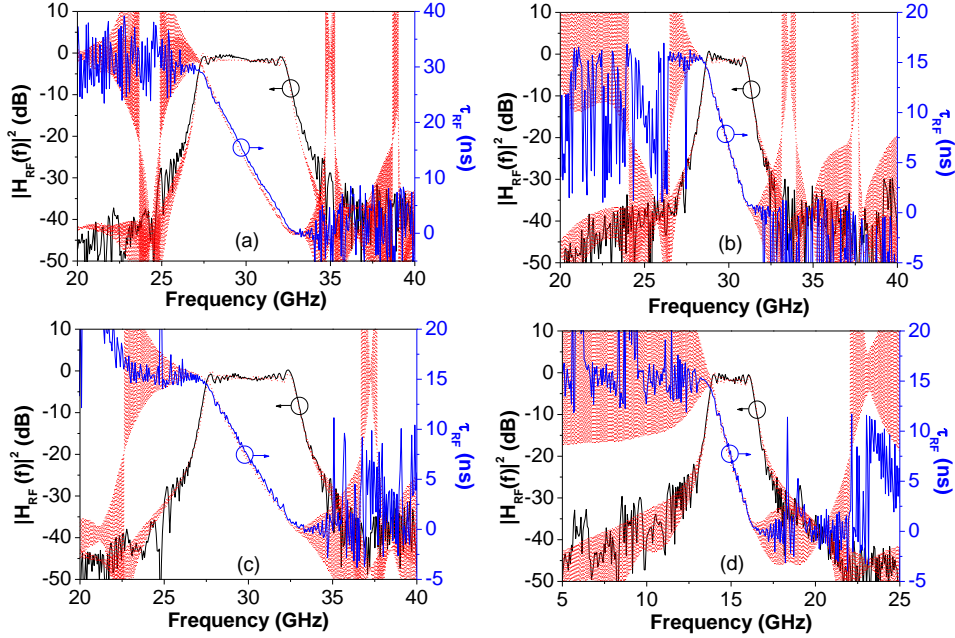
Fig. 5. Amplitude response (black solid line) and electrical delay (blue solid line) obtained experimentally and theoretically (red dot line) for (a) optical source width δλ = 38.4 nm, $\ddot{\varphi}_0 = -1050 \, ps^2$ and Δτ = 199 ps; (b) δλ /2, $\ddot{\varphi}_0$ and Δτ; (c) δλ, $\ddot{\varphi}_0 / 2$ and Δτ/2; (d) δλ, $\ddot{\varphi}_0 / 2$ and Δτ/4.

In the following, we show the capacity of tuning the central frequency of the passband by the adjustment of the VDL in the MZI according to Eq. (6). A 38.4 nm uniform optical source profile was set and two different values of dispersion, $\ddot{\varphi}_0 = -525 \, ps^2$ and $\ddot{\varphi}_0 = -1050 \, ps^2$, were induced in the system. For each case, the optical delay of the MZI is adjusted to obtain the central frequency of the passband within a range of frequencies from 5 to 40 GHz in steps of 2.5 GHz. The experimental results (■,●) are plotted in Fig. 6 and present a linear relationship for each dispersive element with slopes corresponding to both dispersion values of 0.31 and 0.15 GHz/ps, respectively. This linear behaviour was expected from Eq. (6) and the theoretical prediction has been also depicted in Fig. 6 (dashed line), showing an excellent agreement with the experimental results. Note that the passband central frequency can be tuned over a large frequency range since carrier suppression effect is avoided.
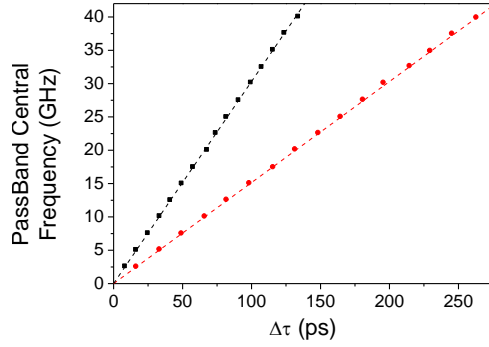
Fig. 6. Experimental relationship between optical delay in MZI and bandpass central frequency for $\ddot{\varphi}_0 = -525\ ps^2$ (■) and $\ddot{\varphi}_0 = -1050\ ps^2$ (●) and the theoretical prediction in dashed line.

In this point, we evaluate the range of the filter bandwidth and chirp values when the central frequency of the filter is fixed. We experimentally demonstrate the dependence of the filter bandwidth and the chirp with the optical bandwidth of the source and the dispersion introduced in the system according to Eqs. (7) and (9), respectively

In the following, the optical source uniform profile was maintained but the optical bandwidth is changed by increasing the number of channels in the OCS. System dispersion is set to $\ddot{\varphi}_0 = -1050\ ps^2$ and $\ddot{\varphi}_0 = -525\ ps^2$ and the central frequency of the passband in each case was around 15 GHz and 30 GHz by means of optical delays in the MZI of 99.3 and 198.1 psec (for $\ddot{\varphi}_0 = -1050\ ps^2$) and 49.5 and 98.2 ps (for $\ddot{\varphi}_0 = -525\ ps^2$). Figure 7 shows the experimental results (●, ■, ▼, ▲) for the different cases. We can observe the relationship between 10-dB bandwidth (BW_{-10dB}) of the passband and the optical bandwidth. The higher system dispersion is, the wider passband is, following a linear behaviour between both magnitudes as predicted in Eq. (7). These magnitudes are characterized by slopes of 0.07 and 0.14 GHz/nm for the tuning frequencies of filter at 15 and 30 GHz, respectively. Note the good agreement of the theoretical simulations (dashed line) in Eq. (7) with the experimental measurements.
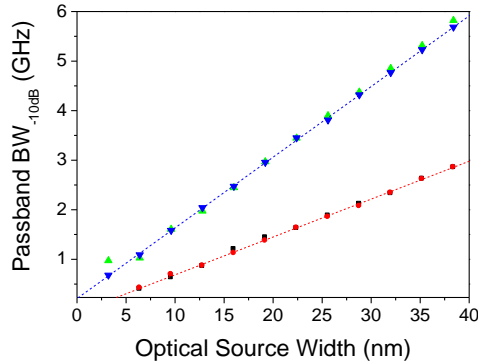

Fig. 7. Experimental relationship between 10-dB bandwidth and optical source width for: $\ddot{\varphi}_0 = -525\ ps^2$, $f_0 = 15$ GHz (●) and $2 \cdot \ddot{\varphi}_0$, f_0 (■); (b) $\ddot{\varphi}_0$, $2 \cdot f_0$ (▼) and $2 \cdot \ddot{\varphi}_0$, $2 \cdot f_0$ (▲). Theoretical simulations (dashed line).

Moreover, as another main advantage over the last microwave photonic filter proposals, the chirp within the passband of the filter in our system can be modified by means of the total dispersion introduced in the system. The optical signal is adjusted to a 38.4 nm width uniform profile and the dispersion induced in the system is changed from −105 to −1575 ps². We

measure the electrical group-delay within the passband generated by the photonic filter when it is tuned at 15 and 30 GHz. Absolute value of the slope of the electrical group-delay (|C|) obtained experimentally in each case (■,•) is shown in Fig. 8 together with the theoretical prediction according to Eq. (9). As can be observed, the higher system dispersion is, the higher chirp is obtained, following a linear behaviour so that filter chirp is incremented in the same order as system dispersion with values from 1.02 to 17.20 and 0.50 to 8.43 ns/GHz for 15 and 30 GHz respectively. We note as |C| is reduced when the central frequency passband is increased as was predicted from Eq. (9). As was previously mentioned, electrical technologies are restricted in terms of frequency operation range as microstrip structures up to 15 GHz or in terms chirp for SIW which present a maximum value of 0.2 ns/GHz. In this way, the structure that we propose in this paper improves both the frequency operation range and passband chirp. Although the system dispersion is introduced by optical fiber links, in order to achieve a compactness solution it can be used different elements as linearly chirped fiber Bragg gratings (LCFBG). Since it is necessary the use of a broadband dispersive element, this structure can be taken advantage of last wideband LCFBG design and fabrication which can operate over 35 nm range [17].
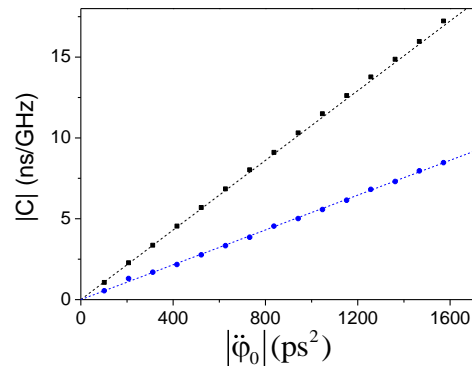

Fig. 8. Experimental results for relationship between first order dispersion ($\left| \ddot{\varphi}_0 \right|$) and filter chirp within passband when it is tuned at 15 GHz (■) and 30 GHz (•). Theoretical prediction for both cases has been added in dashed line.

Finally, as previously shown, we demonstrate the control of the system transfer function by reconfiguring the optical spectrum. As depicted in Fig. 7, the bandwidth of the filter passband can be adjusted by changing the optical bandwidth of the source. In the same way, if the optical power distribution profile is modified, the modulus of the electrical transfer function can be changed. In order to demonstrate it, an apodization factor was applied to the uniform profile (dashed line) as shown in Fig. 9a (solid line), a dispersion of −525 ps^2 and the optical delay of the MZI was adjusted to tune the frequency of the passband at 32.5 GHz. In Fig. 9b, amplitude responses obtained with and without apodization of the optical source are plotted. As can be observed, the shape of the passband has been modified with a significant reduction of the secondary lobes and the avoidance of the ripple existing when a uniform profile is used. Figure 9c shows the corresponding electrical-group delay responses which behaviour is independent on the optical source power distribution. Therefore, we have demonstrated a fully control of the amplitude response of the filter independently of the electrical group-delay characteristic within the passband. Carrier Suppression Effect (CSE) curve has been also depicted in both Figs. 9b and 9c (dotted line), but it does not affect to the filter transfer function, although some nulls are present in the passband, as explained above.
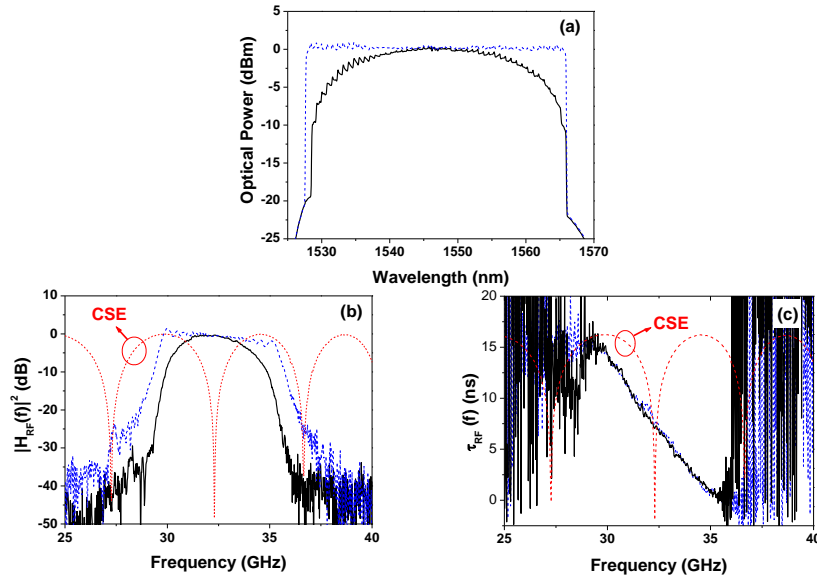
Fig. 9. (a) Optical source power distribution, (b) amplitude response and (c) electrical group-delay response for uniform (dashed line) and apodized (solid line) when passband is tuned around 32.5 GHz. CSE when dispersion is -525 ps^2 (dotted line).

4. Conclusion

In this paper, we have presented a chirped microwave photonic filter based on the amplitude modulation of a broadband optical signal transmitted by a non-linear dispersive element and sliced by a MZI prior to a balanced photodetection. A theoretical analysis has been realized to demonstrate a full reconfiguration of the filter both in terms of the amplitude and phase responses has been probed. The performance of the system has been experimentally demonstrated and theoretically analyzed with an excellent agreement between both results. In this sense, we have shown experimentally as the frequency operation range can be extended up to tens of GHz using DSB modulation since our approach avoids the CSE through the interferometric structure composed by the MZI and the BPD. Indeed, the frequency tuning range of the filter is just limited by the electrical bandwidth of the external modulator and the photodetector. Also, we have evaluated the range of the filter bandwidth and chirp values for a given central frequency. Firstly, we have checked experimentally as the filter bandwidth is determined by the optical bandwidth of the source and the system dispersion. The control over the optical source profile has allowed to change independently the bandwidth of the filter and also the shape of the passband, reducing the secondary lobes and the ripple of the amplitude response. Secondly, we have probed that the chirp range is given by the total system dispersion. A chirp range one order of magnitude higher than previous reported configurations has been experimentally demonstrated achieving maximum values up to tens of ns/GHz at high frequencies. In addition, the balanced photodetection allows to eliminate the baseband component since negative taps are created in the detection itself.

Acknowledgements